VARIABLE FREQUENCY CONTROL OF THE RESONANT HALF BRIDGE DUAL CONVERTER

Quan Li and Peter Wolfs

Central Queensland University

Abstract

The resonant half bridge dual converter has been previously developed for the DC-DC conversion application in a two-stage photovoltaic Module Integrated Converter (MIC). In order to apply Maximum Power Point Tracking (MPPT) for the PV module or provide variable output voltage, the DC-DC converter is required to operate with variable input/output voltage ratios. This paper studies the variable frequency control of the resonant half bridge dual converter, which is able to produce an output voltage range of 1:2.3 while maintaining resonant switching transitions. The design method of the converter is analysed in detail and the explicit control functions for a 200 W converter are established. Both of the theoretical and simulation waveforms are provided. A resonant half bridge dual converter with the voltage clamp is also proposed at the end of this paper.

1. INTRODUCTION

Figure 1 shows the topology for the resonant half bridge dual converter, which is suitable for the DC-DC conversion stage in the photovoltaic (PV) Module Integrated Converter (MIC). It has achieved reasonable efficiency under high switching frequency by operating the converter under Zero-Voltage Switching (ZVS), [1].

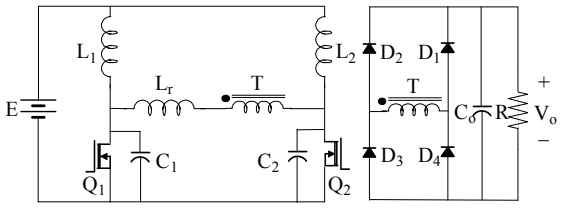

Figure 1. Resonant Half Bridge Dual Converter

In order to apply Maximum Power Point Tracking (MPPT) to the PV module, the resonant half bridge dual converter is required to produce different input/output voltage ratios. The variable frequency control technique can be applied to the Quasi-Resonant Converters (QRC) under different load conditions to maintain the resonant conditions, [2]. Therefore, the same control can be used to achieve variable converter output voltages under the same input voltage for the resonant half bridge dual converter.

This paper studies the variable frequency operation of the resonant half bridge dual converter, which has an input from the photovoltaic source of 20 V, a maximum output of 340 V and 200 W. A full set of design equations are provided and explicit control functions are obtained through the MATLAB program. Both of the theoretical and simulation waveforms at selected points of operation are given and they agree well with each other. A variation of the basic topology with the additional voltage clamp, which has a low switch voltage stress, is also presented at the end of the paper.

2. VARIABLE FREQUENCY OPERATION

The resonance of the converter can be analysed using the equivalent circuit shown in Figure 2. L_r is the effective resonant inductor and C_1 and C_2 are effective resonant capacitors, where $C_1 = C_2 = C$. D_{Q1} and D_{Q2} are embedded reverse body diodes of the mosfets. The current sources (I_0) model L_1 and L_2. Voltage source V_d is the output capacitor voltage reflected to the primary side and Diode D corresponds to the diodes in the output full bridge rectifier. V_d and D reverse if the direction of i_{Lr} reverses.

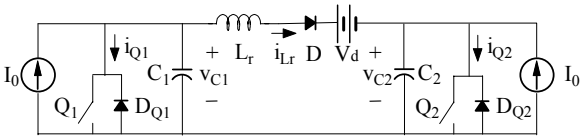

Figure 2. Equivalent Circuit

Before Q_1 turns off, both of Q_1 and Q_2 are closed. Figure 3 shows the four possible states after Q_1 turns off. Equations for the capacitor voltage v_{C1} and the inductor current i_{Lr} in each state are listed in Table 1, where $\omega_0 = 1/\sqrt{L_r C}$ is the angular resonance frequency of the resonant tank. The converter has several operational modes that lead to different average values of the absolute resonant inductor current, which controls the rectifier average current on the secondary side and determines the output power of the converter. A continuous inductor current mode is shown in Figure 13. At t = 0, Q_1 turns off, the converter moves through three states before Q_2 turns off. The initial conditions for State (a) are

$i_{Lr}(0) = -\Delta_1 \cdot I_0$ and $v_{C1}(0) = 0$. State (b) will be momentary in the mode shown in Figure 13 as it does not include a prolonged inductor current zero period and t_2 overlaps with t_1. State (c) exists between t_2 and t_3 when the inductor and the capacitor resonate. State (d) begins once Q_2 or its body diode turns on at t_3.

In the analysis of the converter operation, three parameters are important:

- The timing factor Δ_1, which determines the initial resonant inductor current $i_{Lr}(0) = -\Delta_1 \cdot I_0$ when Q_1 turns off or $i_{Lr}(t_4) = \Delta_1 \cdot I_0$ when Q_2 turns off as shown in Figure 13.
- For discontinuous modes, the delay angle α_d, defined as the angle between the instant when the inductor current falls to zero and the instant when the mosfet turns off as shown in Figure 11.
- The load factor k, defined by the equation $I_0 \cdot Z_0 = k \cdot V_d$, where $Z_0 = \sqrt{L_r / C}$ is the characteristic impedance of the resonant tank made up by the resonant inductor and capacitor.

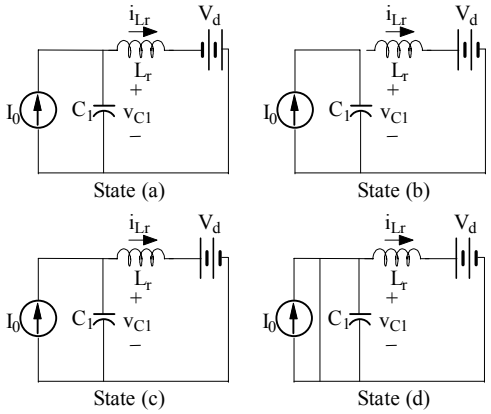

Figure 3. Four Possible States

The timing factor Δ_1, delay angle α_d and load factor k control the operation modes of the converter, [3]. Therefore, the variable load operation of the resonant half bridge dual converter can be realized by varying the timing factor or the delay angle and the load factor, and therefore the switching frequency.

3. THE DESIGN METHOD AND THE CONTROL FUNCTION

3.1 Design equations

The resonant converter has two operation regions: Region 1 where $\Delta_1 = 0$ and $\alpha_d \geq 0$ and Region 2 where $\Delta_1 > 0$. It is required that in both regions $k \geq 1$ to maintain ZVS conditions. The discussion can be started in Region 2. In order to determine the converter parameters the timing factor Δ_1 and the load factor k must be given initially. The design equations are:

$$E \cdot 2I_0 = V_o^2 / R \tag{1}$$

$$V_d \cdot \hat{g}_\Delta(\Delta_1, k) \cdot I_0 = V_o^2 / R \tag{2}$$

$$I_0 \cdot Z_0 = k \cdot V_d \tag{3}$$

$$V_o = N \cdot V_d \tag{4}$$

where E is the input source voltage, V_o is the output load voltage and R is the load resistance. Function $\hat{g}_\Delta(\Delta_1, k)$ is the ratio of the average of the absolute current in the transformer primary, to the input inductor current, I_0 and is determined by two independent variables, Δ_1 and k. From Equations (1) to (4), if E, V_o and R are also known, I_0, V_d, Z_0 and N can be solved. Once the switching frequency is selected, L_r and C can be easily obtained.

3.2 Control functions

After L_r, C and N are fixed, the load factor k is no longer an independent variable affecting V_d or V_o. Then Equation (2) should be rewritten by replacing $\hat{g}_\Delta(\Delta_1, k)$ with $g_\Delta(\Delta_1)$

$$V_d \cdot g_\Delta(\Delta_1) \cdot I_0 = V_o^2 / R \tag{5}$$

Dividing Equation (5) by (1) yields

$$V_d = 2E / g_\Delta(\Delta_1) \tag{6}$$

Equation (6) is the control function for the resonant half bridge dual converter. Unfortunately, function $g_\Delta(\Delta_1)$ cannot be solved directly. An indirect method is to maintain the load factor k as a variable initially in Equation (6) as

$$V_d = 2E / \hat{g}_\Delta(\Delta_1, k) \tag{7}$$

and then to eliminate it by applying the circuit constraint obtained through Equations (1) to (4):

$$k = \frac{N^2 Z_0}{R} \cdot \frac{1}{\hat{g}_\Delta(\Delta_1, k)} \tag{8}$$

Function $\hat{g}_\Delta(\Delta_1, k)$ can be solved numerically by MATLAB program against a range of Δ_1 and k values and the qualified sets of Δ_1 and k values can be picked by the intersection curve of the surface $h_{1,\Delta}(\Delta_1, k) = k$

and the surface $h_{2,\Delta}(\Delta_1,k)=\frac{N^2Z_0}{R}\cdot\frac{1}{\hat{g}_\Delta(\Delta_1,k)}$. The inherent relationship of Δ_1 and k is then established numerically and substituted back to Equation (7) to derive the control function given in Equation (6) in the form of $V_d = M_\Delta(\Delta_1)$ by polynomial fitting.

In Region 1, the analysis of the design method and the control algorithm is similar. All Region 1 equations' counterparts in Region 2 share the same format however the variable Δ_1 needs to be replaced by α_d and the subscript Δ by α to maintain the nomenclatural consistency.

3.3 Design process

As a higher output voltage appears in Region 1, the maximum output voltage, 340 V, must be designed in Region 1 with a non-zero delay angle α_d. Other parameters used in the converter design are $E = 20V$ and $R = 576\Omega$. According to the counterpart of Equation (7), the surface V_d in Region 1 can be drawn against α_d and k in Figure 4, where $0 \le \alpha_d \le 10\,radians$ and $1 \le k \le 10$.

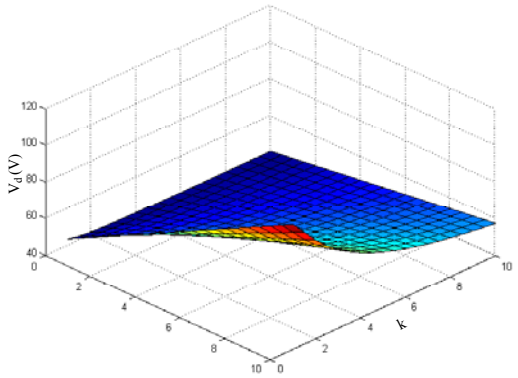

Figure 4. Surface V_d in Region 1

Before selecting the design parameters, special attention must be paid to the peak mosfet voltage and a reasonable voltage level of 200 V is allowed in the design. From Equations (3) and (13), the peak mosfet voltage can be calculated as

$$V_{Q,peak}=\left\{1+\sqrt{k^2+\left[\frac{v_{C1}(t_2)}{V_d}-1\right]^2}\right\}\cdot V_d \qquad (17)$$

From Equations (9) and (11), $v_{C1}(t_2)=V_d$ as $\Delta_1 = 0$ in Region 1 and Equation (17) can be simplified as

$$V_{Q,peak}=(1+k)\cdot V_d \qquad (18)$$

Then the surface $V_{Q,peak}$ can be drawn with a horizontal surface $V_{Q,rating}=200\,V$ in Figure 5 and an initial set of design parameters is selected where $\alpha_d = 4\,radians$ and $k = 2.3$, which limits the peak mosfet voltage to 200 V. The following design process shows that other initial sets of α_d and k values, whose corresponding points fall on the surface $V_{Q,peak}$ and below the surface $V_{Q,rating}$, result in similar or smaller ratios of the maximum to minimum output voltage.

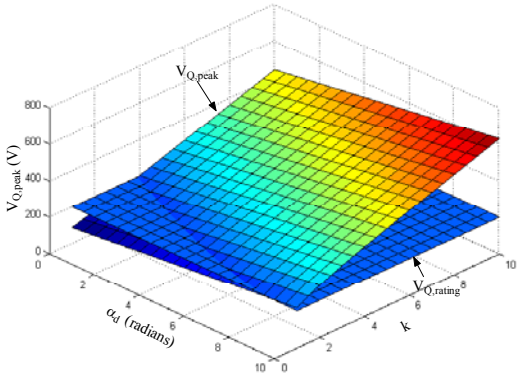

Figure 5. Surfaces $V_{Q,peak}$ and $V_{Q,rating}$

The set of the design equations can be solved and the results are given in Table 2. The resonant inductance and capacitance are not listed here because the switching frequency is not selected. The calculations of these parameters will be conducted later when the range of the switching periods is known.

The circuit constraint or the counterpart of Equation (8) is now applied and the surfaces $h_{1,\alpha}(\alpha_d,k)=k$ and $h_{2,\alpha}(\alpha_d,k)=\frac{N^2Z_0}{R}\cdot\frac{1}{\hat{g}_\alpha(\alpha_d,k)}$ are drawn in Figure 6.

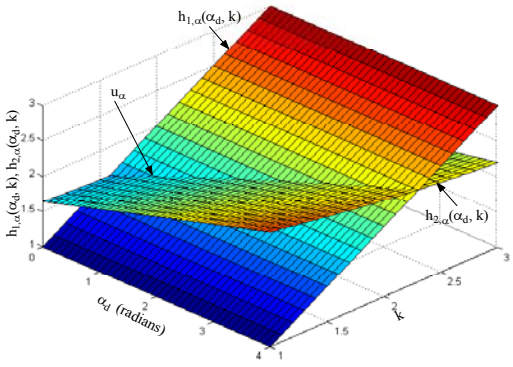

Figure 6. Surfaces $h_{1,\alpha}(\alpha_d,k)$ and $h_{2,\alpha}(\alpha_d,k)$

The intersection curve u_α can be found in Figure 6 and the relationship between α_d and k is back substituted to the control function with the dependent variable given by the counterpart of Equation (7). Through polynomial fitting, the control function $M_\alpha(\alpha_d)$ can be found as

$$V_d = M_\alpha(\alpha_d) = 0.0079\alpha_d^3 + 0.2124\alpha_d^2 + 5.4130\alpha_d + 41.7942 \quad (19)$$

The control function $M_\alpha(\alpha_d)$ is drawn in Figure 7. When α_d reaches zero, Region 1 operation ends and Region 2 operation starts. At this point, $\alpha_d = 0$, $k = 1.59$ and $V_d = 41.8\,V$.

The design process in Region 2 is similar and the surface V_d is drawn against Δ_1 and k in Figure 8, where $0 \le \Delta_1 \le 3$ and $1 \le k \le 10$. It is worth noting that the peak mosfet voltage in Equation (17) is well below 200 V when $k \le 1.59$. The surfaces $h_{1,\Delta}(\Delta_1, k) = k$ and $h_{2,\Delta}(\Delta_1, k) = \frac{N^2 Z_0}{R} \cdot \frac{1}{\hat{g}_\Delta(\Delta_1, k)}$ in the circuit constraint of Equation (8) are drawn in Figure 9. The intersection curve u_Δ can be found and the numerical relationship between Δ_1 and k is back substituted to Equation (7). Through polynomial fitting, the control function $M_\Delta(\Delta_1)$ can be found as:

$$v_d = M_\Delta(\Delta_1) = 0.3005\Delta_1^3 + 0.0221\Delta_1^2 - 9.0395\Delta_1 + 41.7931 \quad (20)$$

The control function $M_\Delta(\Delta_1)$ can be drawn in Figure 10. When $\Delta_1 = 2$, k = 1 and $V_d = 26.2\,V$. A switching frequency of 500 kHz is selected for the lowest output voltage when $\Delta_1 = 2$ and $k = 1$. The angular resonance frequency of the resonant tank and the switching frequency when $\alpha_d = 4\,radians$ and $k = 2.31$ are given in Table 3. The resonant components are $L_r = 6.85\ \mu H$ and $C = 8.82\ nF$.

4. THE THEORECTICAL AND SIMULATION WAVEFORMS

The theoretical waveforms are generated by plotting Equations (9) to (16) at different Δ_1 or α_d and k values and the simulation is performed with SIMULINK. The selected operating points are listed in Table 4 and their corresponding waveforms are shown in Figures 11 to 16.

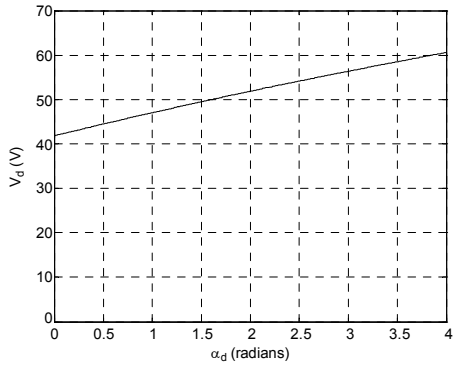

Figure 7. The Control Function $M_\alpha(\alpha_d)$

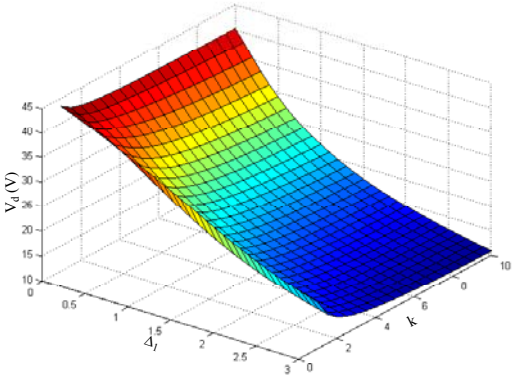

Figure 8. Surface V_d in Region 2

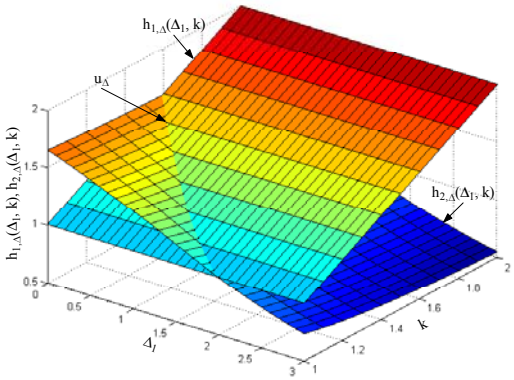

Figure 9. Surfaces $h_{1,\Delta}(\Delta_1, k)$ and $h_{2,\Delta}(\Delta_1, k)$

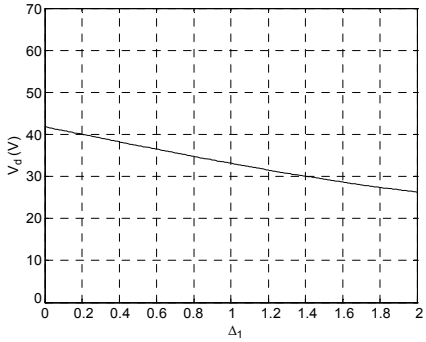

Figure 10. The Control Function $M_\Delta(\Delta_1)$

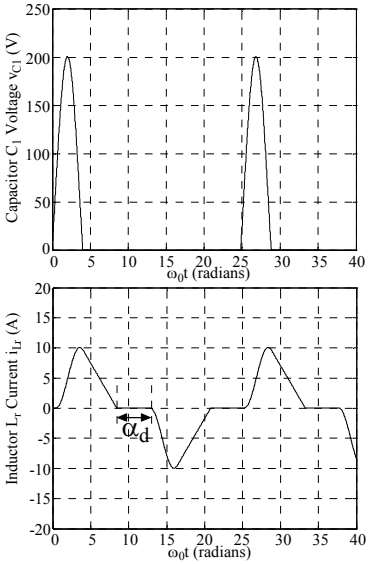

Figure 11. Theoretical Waveforms

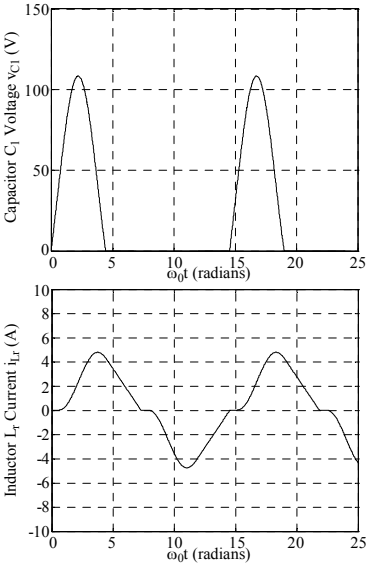

Figure 12. Theoretical Waveforms

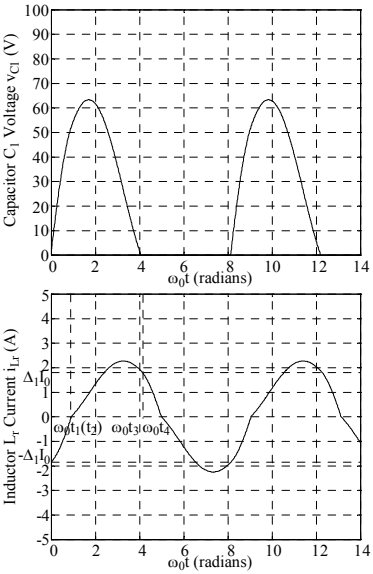

Figure 13. Theoretical Waveforms

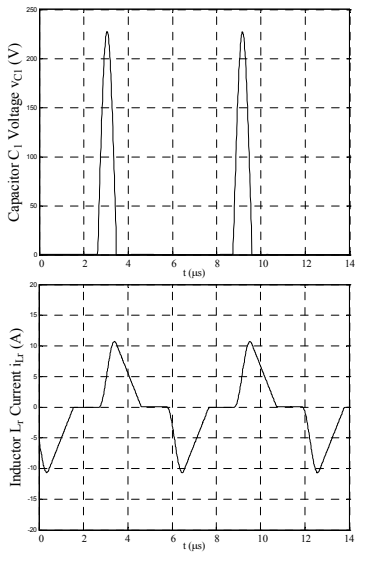

Figure 14. Simulation Waveforms

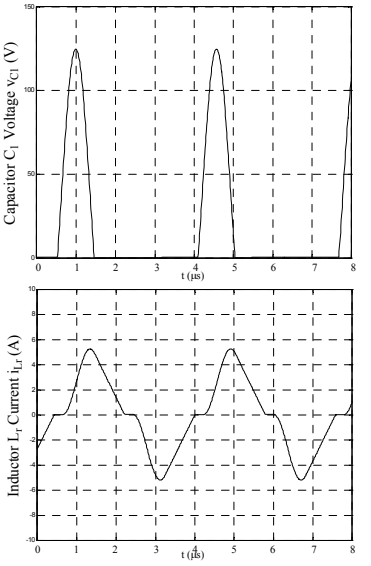

Figure 15. Simulation Waveforms

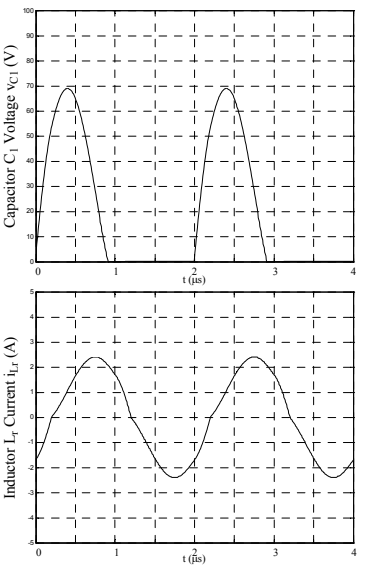

Figure 16. Simulation Waveforms

Figure 17 shows a variation of the resonant half bridge dual converter, which includes a voltage clamping circuit formed by two coupled inductors and two extra diodes. The analysis of this converter is similar to the converter without the voltage clamp. This topology achieves lower voltage stresses across the main switches. However, high returned energy by the clamp windings of the coupled inductors could be a problem and may significantly lower the converter efficiency if no further measures are taken.

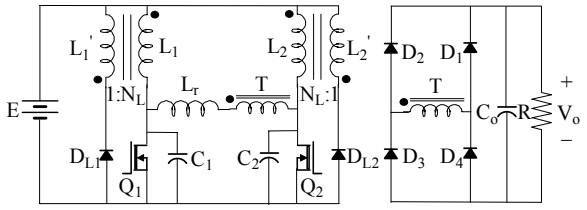

Figure 17. The Resonant Half Bridge Dual Converter with the Voltage Clamp

5. CONCLUSIONS

This paper studies the variable frequency control of the resonant half bridge dual converter based on varying the timing factor Δ_1 or the delay angle α_d and the load factor k. Under variable frequency control, the resonant half bridge dual converter operates with a variable input/output voltage ratio. With a reasonable switch voltage stress, the resonant converter without the voltage clamp is able to achieve a 146 V to 340 V output voltage range. The resonant converter with the voltage clamp has a lower switch voltage stress but a lower efficiency due to the returned energy in the inductor clamp windings.

6. REFERENCES

[1] Q. Li and P. Wolfs, "A Resonant Half Bridge Dual Converter," *Proceedings of Australasian Universities Power Engineering Conference, 2001*, pp. 263-268. *Journal of Electrical & Electronic Engineering Australia*, Vol. 22, No. 1, pp.17-23, 2002.

[2] D. Maksimovic and S. Cuk, "Constant-Frequency Control of Quasi-Resonant Converters," *IEEE Trans. on Power Electron.*, Vol. 6, No. 1, pp. 141-150, Jan. 1991.

[3] P. Wolfs and Q. Li, "An Analysis of a Resonant Half Bridge Dual Converter Operating in Continuous and Discontinuous Modes," *Proceedings of IEEE Power Electronics Specialists Conference, 2002*, pp.1313-1318.

State		Equations	
State (a) $(0 \le t \le t_1)$	v_{C1}	$v_{C1}(t) = (1+\Delta_1)I_0 Z_0 \sin(\omega_0 t) + V_d \cos(\omega_0 t) - V_d$	(9)
	i_{Lr}	$i_{Lr}(t) = (V_d / Z_0)\sin(\omega_0 t) - (1+\Delta_1)I_0 \cos(\omega_0 t) + I_0$	(10)
State (b) $(t_1 \le t \le t_2)$	v_{C1}	$v_{C1}(t) = I_0 / C_1 (t - t_1) + v_{C1}(t_1)$	(11)
	i_{Lr}	$i_{Lr}(t) = 0$	(12)
State (c) $(t_2 \le t \le t_3)$	v_{C1}	$v_{C1}(t) = I_0 Z_0 \sin(\omega_0 t - \omega_0 t_2) + [v_{C1}(t_2) - V_d]\cos(\omega_0 t - \omega_0 t_2) + V_d$	(13)
	i_{Lr}	$i_{Lr}(t) = [(v_{C1}(t_2) - V_d)/Z_0]\sin(\omega_0 t - \omega_0 t_2) - I_0 \cos(\omega_0 t - \omega_0 t_2) + I_0$	(14)
State (d) $(t_3 \le t \le t_4)$	v_{C1}	$v_{C1}(t) = 0$	(15)
	i_{Lr}	$i_{Lr}(t) = i_{Lr}(t_3) - (V_d / L_r)(t - t_3)$	(16)

Table 1. Equations in Each State

I_0 (A)	$\hat{g}_\alpha(\alpha_d, k)$	V_d (V)	N	Z_0 (Ω)	$\omega_0 T_s/2$ (radians)
5.0	0.660	60.6	5.6	27.9	12.4

Table 2. Calculation Results

Δ_1	α_d (radians)	k	$\omega_0 T_s/2$ (radians)	f_s (kHz)	ω_0 (Mrad/s)
2.0	0	1.00	4.07	500	4.07
0	4.0	2.31	12.4	164	

Table 3. Calculation Results

Operating Point	Δ_1	α_d (radians)	k	V_d (V)	Operation Mode	Theoretical Waveforms	Simulation Waveforms
1	0	4.0	2.31	60.5	Discontinuous	Figure 11	Figure 14
2	0	0	1.59	41.8	Discontinuous	Figure 12	Figure 15
3	2.0	0	1.00	26.2	Continuous	Figure 13	Figure 16

Table 4. Selected Operating Points